Nuclear Engineering and Technology 52 (2020) 2678–2685

Contents lists available at ScienceDirect

Nuclear Engineering and Technology

journal homepage: www.elsevier.com/locate/net

Technical Note

Collapse moment estimation for wall-thinned pipe bends and elbows using deep fuzzy neural networks

So Hun Yun, Young Do Koo, Man Gyun Na*

Department of Nuclear Engineering, Chosun University, 309 Pilmun-daero, Dong-gu, Gwangju, 61452, Republic of Korea

ARTICLE INFO

Article history:
Received 15 March 2020
Received in revised form
7 May 2020
Accepted 7 May 2020
Available online 15 May 2020

Keywords:
Collapse moment
Deep fuzzy neural network
Flow accelerated corrosion
Wall-thinning defect

ABSTRACT

The pipe bends and elbows in nuclear power plants (NPPs) are vulnerable to degradation mechanisms and can cause wall-thinning defects. As it is difficult to detect both the defects generated inside the wall-thinned pipes and the preliminary signs, the wall-thinning defects should be accurately estimated to maintain the integrity of NPPs. This paper proposes a deep fuzzy neural network (DFNN) method and estimates the collapse moment of wall-thinned pipe bends and elbows. The proposed model has a simplified structure in which the fuzzy neural network module is repeatedly connected, and it is optimized using the least squares method and genetic algorithm. Numerical data obtained through simulations on the pipe bends and elbows with extrados, intrados, and crown defects were applied to the DFNN model to estimate the collapse moment. The acquired databases were divided into training, optimization, and test datasets and used to train and verify the estimation model. Consequently, the relative root mean square (RMS) errors of the estimated collapse moment at all the defect locations were within 0.25% for the test data. Such a low RMS error indicates that the DFNN model is accurate in estimating the collapse moment for wall-thinned pipe bends and elbows.

1. Introduction

Pipe bends and elbows are important pipe fittings that are used to redirect fluids and increase the structural flexibility of nuclear power plants (NPPs). An elbow is defined according to specific angles in the standard ASME B16.9 [1]. Pipe bends are commonly referred to as bent tubes, and elbows are included in the pipe bends. As pipe bends and elbows are connected to a piping system, the isometric routing can be modified. In addition, by increasing the structural flexibility of the pipe system, the thermal expansion or anchor reaction forces are reduced so that the piping system can behave in the elastic range. In addition, these pipes are capable of absorbing energy through local plastic deformation to ensure that they maintain the integrity of the entire piping system under transient loading conditions such as seismic movement [2].

However, the pipe bends and elbows in NPPs are usually vulnerable to flow-accelerated corrosion (FAC) [3]. FAC is a major degradation mechanism that causes wall-thinning defects. Generally, the vulnerable parts of NPPs are the locations where cracking occurs in the piping system under a high-temperature and high-pressure environment. As wall-thinning defects can steadily grow and cause leakage of piping, the integrity of the pipe bends and elbows is closely related to the safety of the NPPs. The wall-thinning phenomena have been observed in aging NPPs. The management of wall-thinned pipe bends and elbows has been an important concern for securing the safety and reliability of NPPs [4]. As the piping system of NPPs is considered an important component, significant care must be taken not to exceed its collapse moment.

Therefore, this study suggests a method to estimate the collapse moment of wall-thinned pipes accurately under various loading conditions using a deep fuzzy neural network (DFNN) model. The collapse moment was estimated in previous studies by using a subtractive clustering-based fuzzy model [5], support vector machines (SVMs) [6], and fuzzy support vector regression (FSVR) [7]. In this study, the proposed DFNN model for estimating the collapse moment demonstrated lower relative root mean square (RMS) errors overall than those of the previous studies.

Data related to the collapse moment should be provided and trained to develop and test the DFNN model. These data had been obtained by performing finite element analyses (FEAs), assuming wall-thinning defects of various sizes on extrados, intrados, and

* Corresponding author.
E-mail address: magyna@chosun.ac.kr (M.G. Na).

https://doi.org/10.1016/j.net.2020.05.006

crown [5]. Moreover, various loading conditions and defect geometries were considered. These conditions were applied to the DFNN model as the input signals to estimate the collapse moment.

2. DFNN methodology

2.1. DFNN structure

The DFNN model not only has the capabilities of neural networks but also considers the human-like thinking and reasoning of fuzzy logic systems [8]. A fuzzy inference system (FIS) uses fuzzy rules to deal with the ambiguity of data, and neural networks have the ability to learn by weighing the data. The fusion of these two systems is a powerful tool that enables the realization of intelligence close to human thinking. It has been called a fuzzy neural network (FNN), considering that the internal structures of these two systems are similar and can be combined [9]. In addition, FNN modules are repeatedly connected in the proposed DFNN model, which helps improve the robustness of the model over that of a single FNN model [10]. Fig. 1 shows the architecture of the DFNN model. Input x is applied to each FNN module, and the final optimized $\hat{y}_g$ is derived from the g^{th} FNN module. $y_1, y_2, \cdots, y_g$ are the outputs calculated at each FNN module, and they are used as another input in the next module. The output is optimized through the connected structure.

The input and output pairs are trained in the DFNN model. As these values are real-valued variables, a Takagi–Sugeno-type FIS, which does not require a defuzzifier at the output terminal, is used [11]. Fig. 2 shows the Takagi–Sugeno-type FIS, which can be expressed as Eq. (1).

$$R_i\left(i^{th}\text{ fuzzy rule}\right): \text{If } x_1(k) \text{ is } G_{i1}(k) \text{ AND } \cdots \text{ AND } x_m(k) \text{ is } G_{im}(k), \text{ then } y^i(k) \text{ is } f^i(x_1(k), \cdots, x_m(k)), \tag{1}$$

where $x_j(k)$ is the input variable to the FIS ($j = 1, 2, \cdots, m$; $m =$ the number of input variables), $G_{ij}(k)$ is the membership function of the j^{th} input values of the i^{th} fuzzy rule ($i = 1, 2, \cdots, n$; $n =$ the number of rules), and f^i is the output of the i^{th} fuzzy rule.

Each FNN module consists of six layers containing fuzzy inference and learning units. The first FNN module is illustrated in Fig. 3. This module includes fuzzy rules, membership functions, and normalization. Therefore, the output from the FNN module is defined as Eq. (2).

$$\hat{y}(k) = \sum_{i=1}^{n} \alpha^i(k) f^i(x_1, x_2, \cdots, x_m), \tag{2}$$

where $\alpha^i(k)$ is a normalized weighting value of the i^{th} fuzzy rule output.

The membership function defines the degree of membership of an element in a fuzzy set, which is in the range of [0, 1]. Membership functions have several shapes [12]. In this study, the symmetric Gaussian membership function is used and is given in Eq. (3). The Gaussian membership function has the advantage of being smooth and nonzero at all points.

$$G_{ij}\left(x_j(k)\right) = e^{-\left(x_j(k)-c_{ij}\right)^2 / 2s_{ij}^2}. \tag{3}$$

In Eq. (3), c_{ij} represents the center position of the Gaussian function for the i^{th} rule and the j^{th} input, and s_{ij} represents the sharpness of the Gaussian function for the i^{th} rule and the j^{th} input. Therefore, the i^{th} rules of each step of the continuously connected FNN modules are expressed as Eq. (4).

$$\begin{aligned}
&\text{the first FNN module}\\
&\begin{bmatrix}\text{If } x_1(k) \text{ is } G_{i1}^1(k) \text{ and } \cdots, x_m(k) \text{ is } G_{im}^1(k),\\ \text{then } \hat{y}_1^i(k) \text{ is } f_1^i(x_1(k), \cdots, x_m(k))\end{bmatrix}\\
&\text{the second FNN module}\\
&\begin{bmatrix}\text{If } x_1(k) \text{ is } G_{i1}^2(k) \text{ and } \cdots, x_m(k) \text{ is } G_{im}^2(k), \text{ and } \hat{y}_1(k) \text{ is } G_{i(m+1)}^2(k),\\ \text{then } \hat{y}_2^i(k) \text{ is } f_2^i(x_1(k), \cdots, x_m(k), \hat{y}_1(k))\end{bmatrix}\\
&\quad\vdots\\
&(g-1)^{th}\text{ FNN module}\\
&\begin{bmatrix}\text{If } x_1(k) \text{ is } G_{i1}^{g-1}(k) \text{ and } \cdots, x_m(k) \text{ is } G_{im}^{g-1}(k), \text{ and } \hat{y}_{g-2}(k) \text{ is } G_{i(m+1)}^{g-1}(k),\\ \text{then } \hat{y}_{g-1}^i(k) \text{ is } f_{g-1}^i\left(x_1(k), \cdots, x_m(k), \hat{y}_{g-2}(k)\right)\end{bmatrix}\\
&g^{th}\text{ FNN module}\\
&\begin{bmatrix}\text{If } x_1(k) \text{ is } G_{i1}^g(k) \text{ and } \cdots, x_m(k) \text{ is } G_{im}^g(k), \text{ and } \hat{y}_{g-1}(k) \text{ is } G_{i(m+1)}^g(k),\\ \text{then } \hat{y}_g^i(k) \text{ is } f_g^i\left(x_1(k), \cdots, x_m(k), \hat{y}_{g-1}(k)\right)\end{bmatrix}.
\end{aligned} \tag{4}$$

The i^{th} fuzzy rule output at the g^{th} FNN module is expressed as Eq. (5) and the result of the g^{th} FNN module, the final output, is expressed as Eq. (6).

$$f_g^i\left(x_1(k), \cdots, x_m(k), \hat{y}_{g-1}(k)\right) = \sum_{j=1}^{m} q_{ij} x_j + q_{i(m+1)} \hat{y}_{g-1} + r_i, \tag{5}$$

where q_{ij} is the weight of the i^{th} fuzzy input variable and r_i is the bias of the i^{th} fuzzy rule. q_{ij} and r_i are called consequent parameters because they appear in the consequent part of the "if/then" rule.

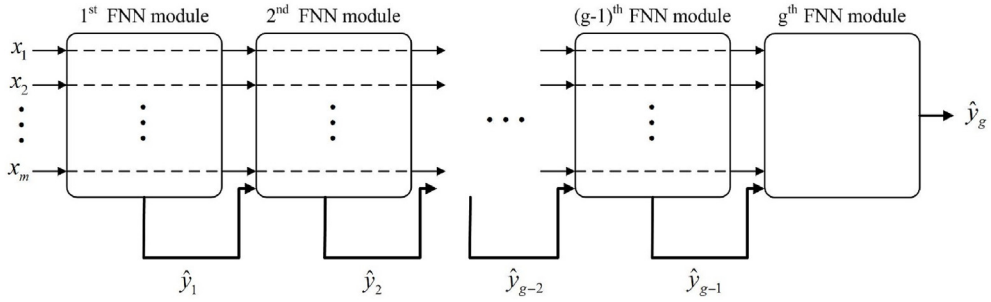

Fig. 1. Structure of the DFNN model.

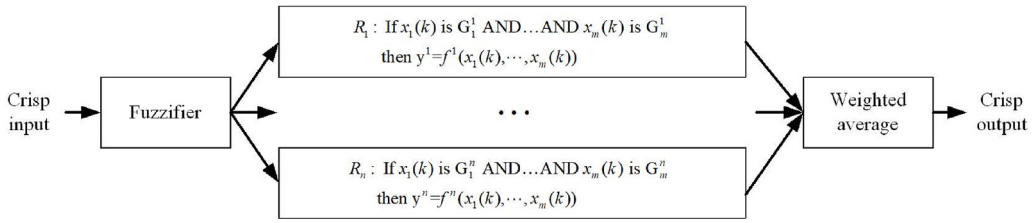

Fig. 2. Takagi–sugeno-type FIS.

$$\hat{y}_g(k)=\sum_{i=1}^{n}\alpha_g^i(k)f_g^i\left(x_1,x_2,\cdots,x_m,\hat{y}_{g-1}(k)\right), \tag{6}$$

where $\alpha_g^i(k)$ is a normalized weighting value of the i^{th} fuzzy rule output at the g^{th} FNN module.

2.2. Optimization of DFNN model

The proposed DFNN model is optimized using a genetic algorithm and the least squares method. Fig. 4 shows the optimization of the DFNN model during the training process. A genetic algorithm searches for global optimum solutions by gradually improving theories that mimic genetic and evolutionary mechanisms [13]. As genetic algorithms generate initial random chromosomes and generation proceeds, chromosome populations are repeatedly changed by mechanisms inspired by natural evolution, such as selection, crossover, and mutation. The genetic algorithm determines whether each chromosome in a population is appropriate for a given objective and assesses the appropriateness. Therefore, a fitness function is required for assigning their scores, and the genetic algorithm attempts to maximize this function. The fitness function was intended to minimize the RMS and maximum errors in the genetic algorithm, as shown in Eq. (7). The weighting function of the errors is optimized to reduce the residuals between the actual measured values and the values estimated using the DFNN model.

$$F=\exp(-\lambda_1E_1-\lambda_2E_2-\lambda_3E_3-\lambda_4E_4), \tag{7}$$

where λ_1, λ_2, λ_3, and λ_4 are the weighting coefficients, and E_1, E_2, E_3, and E_4 are correlated with the estimation errors and are expressed, respectively, as

$$E_1=\sqrt{\frac{1}{N_T}\sum_{k=1}^{N_T}(y_t(k)-\hat{y}_t(k))^2},$$

$$E_2=\sqrt{\frac{1}{N_O}\sum_{k=1}^{N_O}(y_o(k)-\hat{y}_o(k))^2},$$

$$E_3=\max|y_t(k)-\hat{y}_t(k)|,$$

$$E_4=\max|y_o(k)-\hat{y}_o(k)|.$$

The subscripts t and o represent the training and optimization data, respectively. Thus, the variables N_T and N_O indicate the numbers of the training and optimization data, respectively. Furthermore, $y(k)$ and $\hat{y}(k)$ used as outputs of each FNN modules indicate the target values calculated using the FEA, and the estimated values derived using the DFNN model. The antecedent parameters c_{ij} and s_{ij} included in the membership function are determined by the genetic algorithm, and the consequent parameters are optimized by the least squares method. The consequent parameters are calculated to minimize the objective function by the squared error between the target and estimated values, as expressed by Eq. (8).

$$J=\sum_{k=1}^{N_T}(y(k)-\hat{y}(k))^2=\frac{1}{2}(\mathbf{y}-\hat{\mathbf{y}})^2. \tag{8}$$

The optimum number of FNN modules is determined so that the fitness function does not decrease distinctly as the FNN modules are added.

3. Data applied to DFNN

The results obtained in a previous study [5] were used to develop the DFNN model. Fig. 5 shows the vertical and horizontal cross-sections of the modeled pipes and the parameters of the wall-thinned pipe bends and elbows used in this study. The collapse moment is used as an indicator of the load carrying capacity of the structure to avoid exceeding the design limits of the pipes [14]. Therefore, this parameter was obtained to evaluate the collapse load of the wall-thinned pipe bends and elbows, which was estimated using the proposed DFNN model.

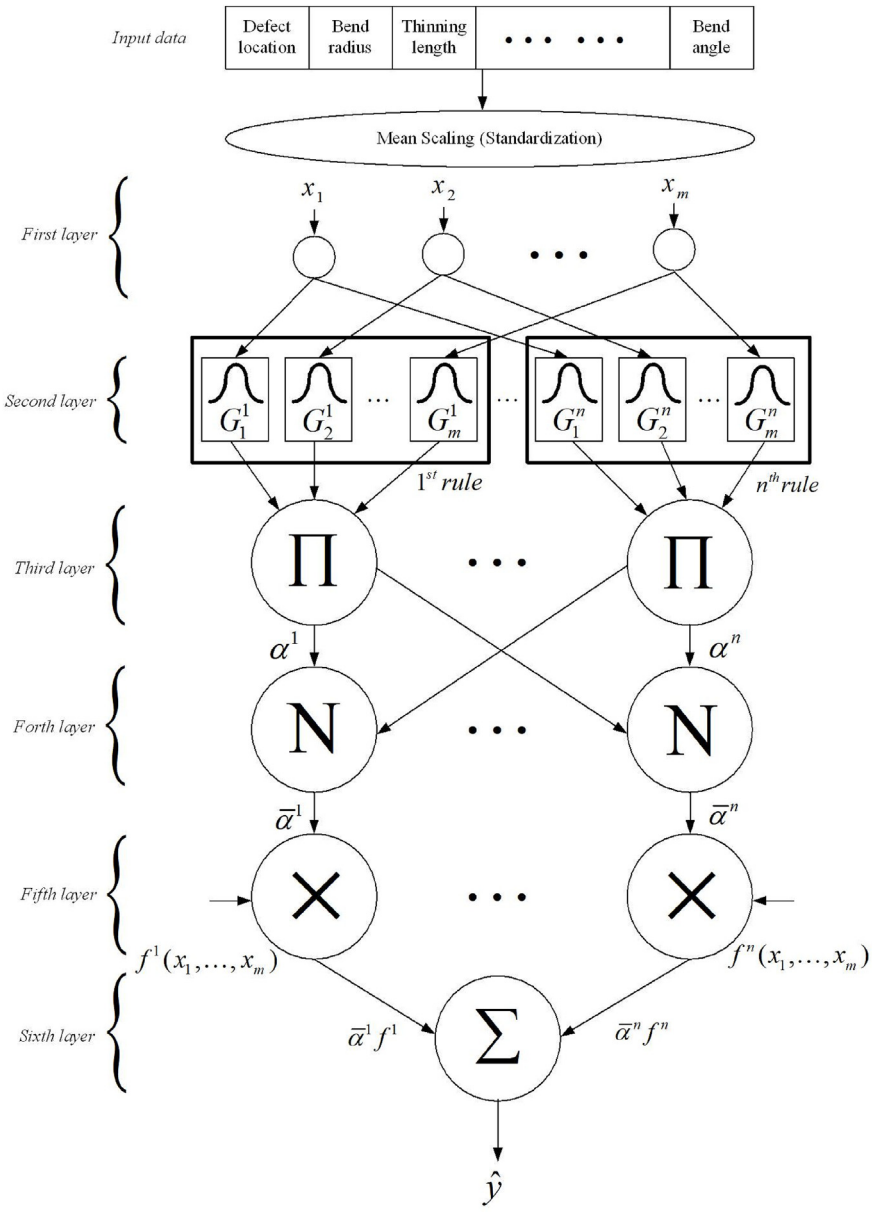

Fig. 3. First FNN module.

The model of pipe bends and elbows was considered to be representative geometry, as summarized in Table 1. Carbon steel bends having a diameter (D_o) of 400 mm and a nominal thickness (t_{nom}) of 20 mm were used. R_b and R_m, which indicate the radii of the curvature and pipe, respectively, represent the geometry of the elbow. Then, the dimensionless bend radius ratio (R_b/R_m) was used with the values of 3 and 6 in this study. The length of the straight pipe connected to the elbow was $10R_m$ to permit free ovalization of the end section of the bends. The bend angles (ϕ) of the pipe bends and elbows were considered to be 30°, 60°, and 90°. The wall-thinning defects of the pipe bends and elbows are located in the extrados, intrados, and crown. The variables representing the wall-thinning defects are L_s, θ, and t_p. L_s represents the thinning length, 2θ is the circumferential angle of the thinning defect, and t_p is the minimum thickness from the thinned defect area.

In addition, the applied load in FEAs is the result of the combination of bending load and internal pressure as shown in Table 2 [5]. The internal pressure was set within a range of 0–20 MPa. The bending loads of the opening and closing modes in the in-plane direction were considered. The yield stress and ultimate tensile stress of the specific material of the bend and attached pipes were 302 MPa and 452 MPa, respectively. The elastic modulus and Poisson's ratio were 206 GPa and 0.36, respectively.

As shown in Table 3, representative values were selected. The defects existing inside the pipe were located at the center line of the extrados, intrados, and crown of the pipe bends and elbows, and the axial and circumferential defects were assumed to be circular. The pipe bends and elbows had approximately 23.3%, 46.6%, and 69.9% wall-thinning defects compared with the existing thickness, and the thinning lengths were considered to be 0.25, 0.5, 1.0, 1.5, and 2 times the diameter of the pipe. θ/π values were used as the dimensionless number. When θ/π becomes 1, it indicates that thinning occurred in the circumferential direction as a whole. Accordingly, the dimensionless thinning angles θ/π were selected within the range of 0–0.5, with the representative values being 0.0625, 0.125, 0.25, and 0.5.

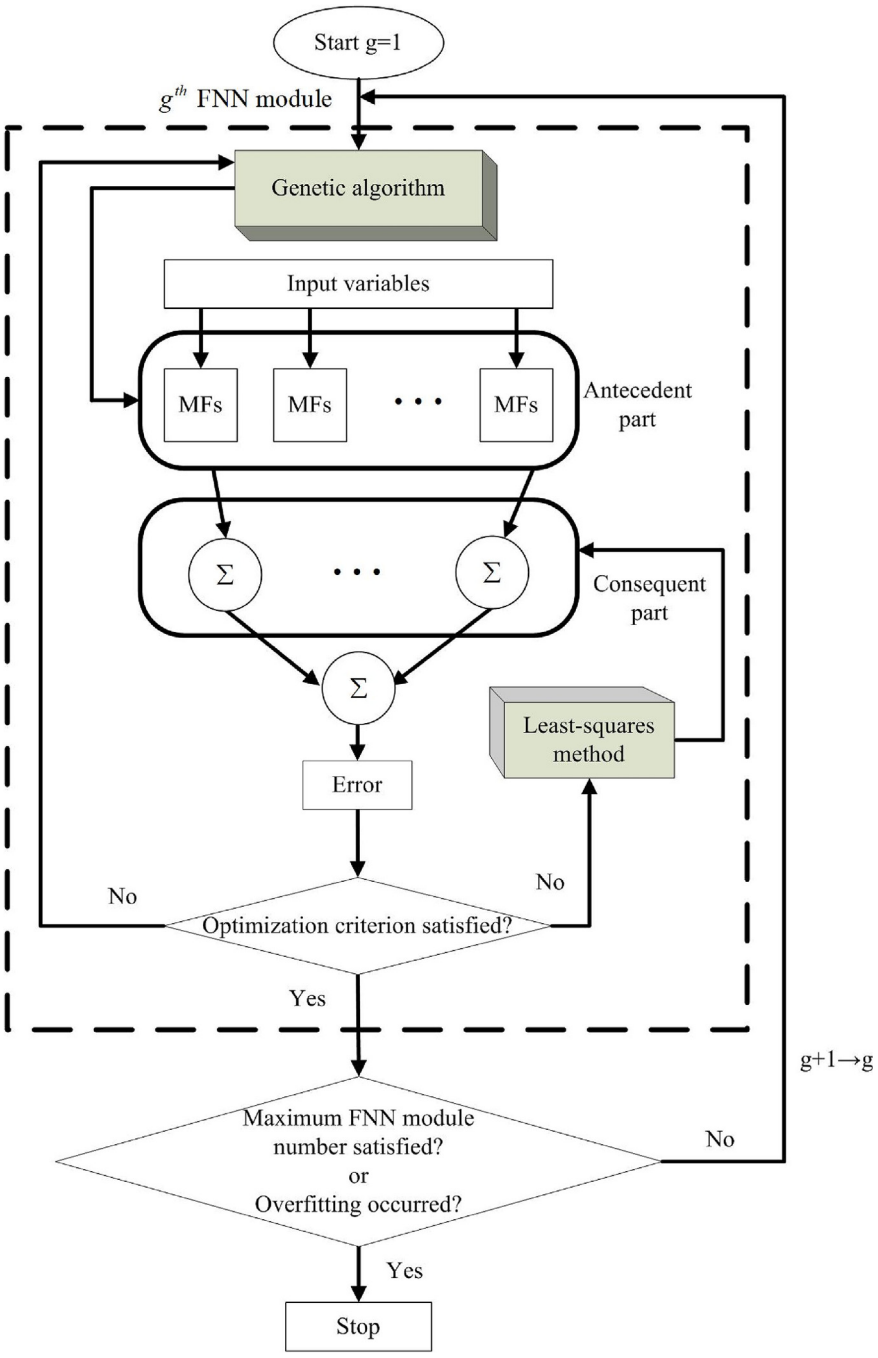

Fig. 4. DFNN optimization procedure.

The acquired data consist of a total of 3712 input–output data pairs $(x_1, x_2, \cdots, x_8, y_t)$ for 1700 extrados and intrados defect location cases, and 312 crown cases. The characteristics of the collapse moment were distinguished using the wall-thinning position, which is expressed by x_1. Therefore, three DFNN models were designed to classify the three wall-thinning defect locations. The input signals x_2 through x_8 indicate the bend radius, thinning length, thinning angle, wall thickness at the thinning defect, internal pressure, bending modes of opening and closing, and bend angle, respectively. y_t is the collapse moment value, which is the target value to be estimated.

4. Experimental results and discussion

The process of calculating the collapse moment by performing the FEAs requires a high level of computation and analysis and takes a very long time. Therefore, the DFNN model was applied to estimate the collapse moment obtained through the FEAs. By training the DFNN model with the database for the wall-thinned pipe bends and elbows, the collapse moment values can be estimated easily and quickly instead of performing FEAs.

The entire dataset obtained was divided into training, optimization, and test datasets. The training and optimization datasets were used to develop the DFNN model. The test dataset was independent of

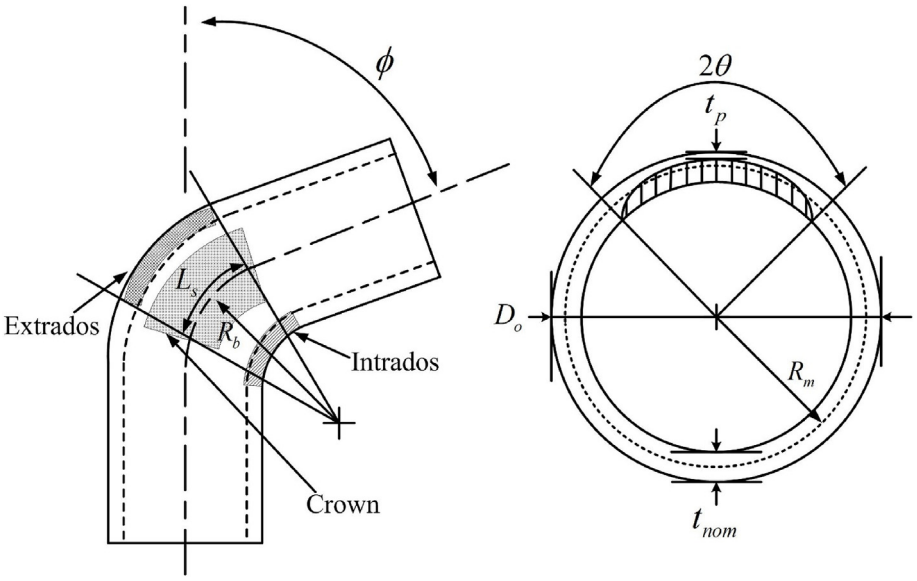

Fig. 5. Schematic illustrations of the wall-thinned defects in the pipe bends and elbows.

Table 1
Conditions of the FEA for the pipe bends and elbows.

Diameter (D_o)	400 mm
Nominal thickness (t_{nom})	20 mm
Length of straight pipe connected to the elbow	$10R_m$
Bend radius (R_b/R_m)	3, 6
Bend angle (ϕ)	30°, 60°, 90°

Table 2
Combined load conditions.

Bending mode	Opening and closing
Pressure (MPa)	0, 5, 10, 15, 20

Table 3
Geometry of the wall-thinning defects considered in FEA (refer to the symbols in Fig. 5).

Wall-thinned locations	Extrados, Intrados, Crown
Thinning length (L_s/D_o)	0.25, 0.5, 1.0, 1.5, 2.0
$(t_{nom} - t_p)/t_{nom}$	0.233, 0.466, 0.699
θ/π	0.0625, 0.125, 0.25, 0.50

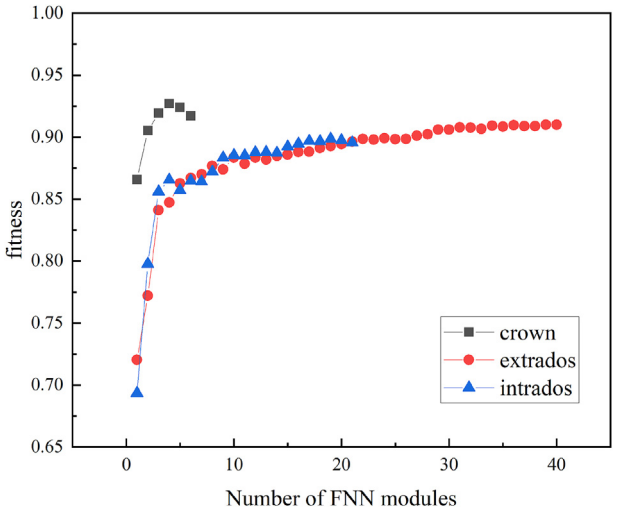

Fig. 6. Fitness function values versus the number of FNN modules.

Table 4
Performance of collapse moment estimation using DFNN.

Defect location	Rule number	FNN module number	Development data		Test data	
			Relative RMSE (%)	Relative max. error (%)	Relative RMSE (%)	Relative max. error (%)
Extrados	2	22	0.5265	2.3901	0.3781	1.5389
	5	18	0.3701	1.7322	0.2530	0.6743
	10	**40**	**0.1780**	**0.7931**	**0.1897**	**0.7313**
	15	13	0.2429	1.1249	0.2053	0.7199
	20	18	0.1897	0.9094	0.1878	0.5965
Intrados	2	11	0.8594	4.3371	0.4977	1.2717
	5	29	0.3403	1.8125	0.2828	0.9743
	10	26	0.2688	1.3183	0.2354	0.7333
	15	**20**	**0.2428**	**1.2202**	**0.2092**	**0.6814**
	20	27	0.1963	0.9645	0.2179	0.7240
Crown	2	17	0.1714	0.5367	0.2199	0.6794
	3	32	0.0930	0.3532	0.2639	1.0679
	5	20	0.0931	0.3545	0.2049	0.6245
	7	14	0.0937	0.3224	0.1964	0.6338
	9	**5**	**0.1409**	**0.4483**	**0.1930**	**0.5617**
	11	6	0.1088	0.3555	0.2034	0.7544

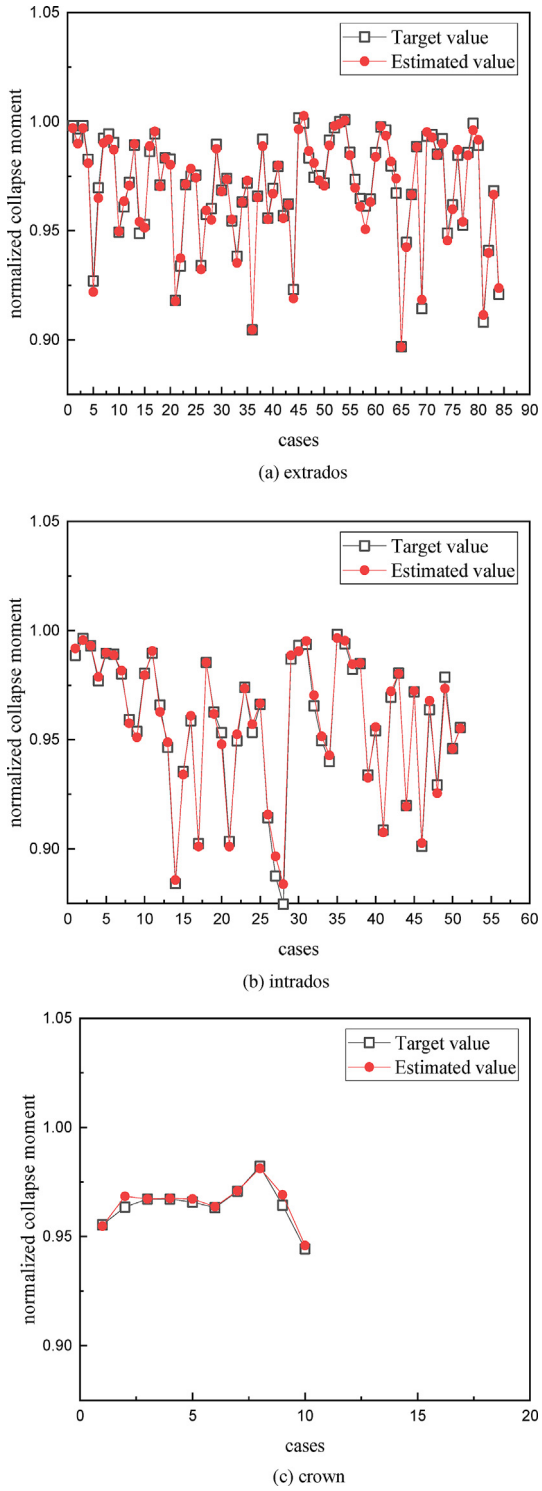

Fig. 7. Results of collapse moment estimation for test data: (a) extrados, (b) intrados, and (c) crown.

the development dataset and was used to verify the developed model. The development (training and optimization) data were selected using a subtractive clustering method [15] from all the acquired data so that data with good information would be used for training and optimizing the proposed DFNN model. RMS error was used to assess the results of the DFNN model. Table 4 summarizes the estimation results of the DFNN model by the relative RMS error. The relative RMS error for the test dataset at the extrados defects was 0.1897%. The relative RMS error for the test dataset at the intrados defects was 0.2092%. The relative RMS error for the test dataset at the crown defects was 0.1930%. Fig. 6 shows that the fitness function values increase gradually as the number of FNN modules increases. As shown in Table 4, the optimum numbers of FNN modules are 40, 20, and 5 for the extrados, intrados, and crown defects, respectively. These optimum module numbers were determined so that the overfitting phenomena would not occur. The number of FNN modules is small for crown defects because the amount of acquired data is small. The proposed method estimated the collapse moment accurately within the relative RMS error of less than 0.25% overall. The error levels for the three defect locations are almost the same.

Fig. 7 shows the target and estimated collapse moments for the test dataset used in the DFNN model for the extrados, intrados, and crown defects. Comparing the target and estimated collapse moments at all locations, the DFNN model accurately estimated the independent test data and the trained data. Fig. 8 shows the error histograms for the extrados defects, and similar graphs can be obtained for the intrados and crown defects.

In addition to evaluating the performance of the proposed methodology, we compared the proposed algorithm with other algorithms developed in the existing literature. Previously, fuzzy,

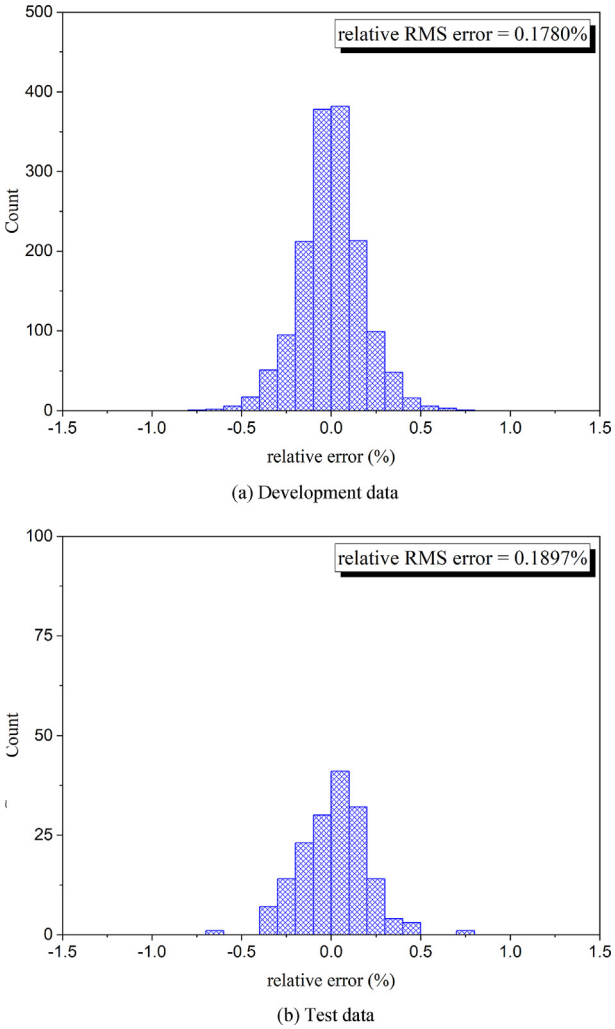

Fig. 8. Estimation error histograms for the extrados defects: (a) development data and (b) test data.

Table 5
Comparison of the proposed DFNN model with previously studied algorithms [5–7].

Defect location	Proposed DFNN model		Fuzzy model		SVR model		FSVR model	
	Test data		Test data		Test data		Test data	
	Relative RMSE (%)	Relative max. error (%)	Relative RMSE (%)	Relative max. error (%)	Relative RMSE (%)	Relative max. error (%)	Relative RMSE (%)	Relative max. error (%)
Extrados	0.1897	0.7313	0.8095	4.5134	0.4985	1.7341	0.2543	0.6529
Intrados	0.2092	0.6814	0.9354	6.0006	0.5293	1.5878	0.2703	0.8703
Crown	0.1930	0.5617	0.7841	2.3344	0.0850	0.1261	0.1540	0.4050

SVM, and FSVR models were developed using the same data as in this study [5–7]. The performance of each model is shown in Table 5. The proposed DFNN model performs better than the other methods in some aspects.

The SVM finds the optimal linear decision boundary that separates data linearly. It is used to classify learning data. However, support vector regression (SVR), which introduces an ε-insensitive loss function to the regression model of the SVM, is used to extend the range of regression problems to estimate arbitrary real values [16]. SVM shows good generalization performance with a small amount of learning data due to structural risk minimization whereas learning theories such as neural networks are based on empirical risk minimization [17]. The number of 312 acquired data for crown defects is relatively much smaller than 1700 data for extrados and intrados defects, respectively. Therefore, the SVM and FSVR models performed slightly better for crown defects with a small dataset than for the extrados and intrados defects. However, the DFNN model with deeply connected FNN modules could be effectively used to train large amounts of data. The DFNN model showed an RMS error less than 1.22% at all locations. In particular, the estimation values of the DFNN for the extrados and intrados defects were more accurate than those of the other methodologies. The DFNN model, in which the FNN module is connected sequentially, will continue to provide useful information, thereby leading to more accurate results.

5. Conclusions

In this study, DFNN models were developed to estimate the collapse moment for the wall-thinned pipe bends and elbows in the piping system of NPPs. The results of FEA were used as a dataset for training the DFNN models. Various loading conditions were considered, and the wall-thinning defects were assumed at the extrados, intrados, and crown locations. The developed model was trained and verified with separate development and test datasets. For all the defects, the relative RMS errors for the development and test data were within approximately 0.25% and approximately 0.21%, respectively. The developed DFNN models accurately estimated the collapse moment of the wall-thinned pipe bends and elbows. Therefore, the suggested DFNN model can be effectively applied to estimate the wall-thinning state of the pipe bends and elbows by estimating the collapse moment easily and quickly.

Declaration of competing interest

The authors declare that they have no known competing financial interests or personal relationships that could have appeared to influence the work reported in this paper.

Acknowledgments

This study was supported by research fund from Chosun University, Republic of Korea (2017).

References

[1] ASME, Factory-made Wrought Buttwelding Fittings, B16.9, American Society of Mechanical Engineers, New York, USA, 2001.
[2] M.G. Na, J.W. Kim, Effect of bend angle on the collapse behavior of locally wall thinned pipe bends, Transactions of the KSME, A 30 (2006) 1269–1275.
[3] M. El-Gammal, H. Mazhar, J.S. Cotton, C. Shefski, J. Pietralik, C.Y. Ching, The hydrodynamic effects of single-phase flow on flow accelerated corrosion in a 90-degree elbow, Nucl. Eng. Des. 240 (2010) 1589–1598.
[4] W.H. Ahmed, Flow accelerated corrosion in nuclear power plants, in: A. Wael (Ed.), Nuclear Power-Practical Aspects, InTech, 2012.
[5] M.G. Na, J.W. Kim, I.J. Hwang, Estimation of collapse moment for the wall-thinned pipe bends using fuzzy model identification, Nucl. Eng. Des. 236 (2006) 1335–1343.
[6] M.G. Na, J.W. Kim, I.J. Hwang, Collapse moment estimation by support vector machines for wall-thinned pipe bends and elbows, Nucl. Eng. Des. 237 (2007) 451–459.
[7] H.Y. Yang, M.G. Na, J.W. Kim, Fuzzy support vector regression model for the calculation of the collapse moment for wall-thinned pipes, Nucl. Eng. Technol. 40 (2008) 607–614.
[8] Y. Zhang, H. Ge, Freeway travel time prediction using Takagi-Sugeno-Kang fuzzy neural network, Comput. Aided Civ. Infrastruct. Eng. 28 (2013) 594–603.
[9] M.S. Jang, D.C. Jang, Design of artificial neural networks for fuzzy control system, The Transactions of the Korea Information Processing Society 2 (1995) 626–633.
[10] J. Kamruzzaman, Y. Kumagai, H. Hikita, A cascaded artificial neural network architecture with novel robustness, in: Proceedings Singapore ICCS/ISITA92, IEEE, 1992, pp. 1235–1239.
[11] T. Takagi, M. Sugeno, Fuzzy identification of systems and its applications to modeling and control, IEEE Trans. Syst. Man Cybern. SMC-15 (1985) 116–132.
[12] J. Zhao, B.K. Bose, Evaluation of membership functions for fuzzy logic controlled induction motor drive, in: IEEE 2002 28th Annual Conference of the Industrial Electronics Society, IECON 02. IEEE, 2002, pp. 229–234.
[13] D.E. Goldberg, Genetic Algorithms in Search, Optimization and Machine Learning, Addison-Wesley Longman Publishing Co., Inc., USA, 1989.
[14] H.M. Mourad, Elastic-plastic behavior and limit load analysis of pipe bends under out-of-plane moment loading and internal pressure, Thesis for Master of Science in Engineering, American University in Cairo, 1999.
[15] S.L. Chiu, Fuzzy model identification based on cluster estimation, J. Intell. Fuzzy Syst. 2 (1994) 267–278.
[16] V. Vapnik, The Nature of Statistical Learning Theory, Springer, New York, 1995.
[17] H. Li, Y. Liang, Q. Xu, Support vector machines and its applications in chemistry, Chemometr. Intell. Lab. Syst. 95 (2009) 188–198.